METEOROLOGICAL APPLICATIONS
*Meteorol. Appl.* **24**: 43–51 (2017)
Published online 29 December 2016 in Wiley Online Library
(wileyonlinelibrary.com) DOI: 10.1002/met.1603

RMetS
Royal Meteorological Society

# The use of a numerical weather prediction model to simulate the release of a dense gas with an application to the Lake Nyos disaster of 1986

R. R. Burton,[a]* J. Dudhia,[b] A. M. Gadian[a] and S. D. Mobbs[a]
[a] *National Centre for Atmospheric Science, University of Leeds, UK*
[b] *National Center for Atmospheric Research, Boulder, CO, USA*

**ABSTRACT:** The spread of a dense gas in the atmosphere is a phenomenon that occurs widely with natural (and anthropogenic) causes and is often associated with high impact and hazardous events. In this study a method of simulating the spread of dense gases in a numerical weather prediction model is presented. This approach has the advantage that dense gases can be simulated in regions of complex terrain using realistic forcings (in terms of both the driving meteorological fields and the representation of surface characteristics). The model formulation is tested against semi-idealized gravity-current-type experiments and similar modelling studies. As an example application, the Lake Nyos disaster of 1986, where a dense $CO_2$ cloud spread through a mountainous region of Cameroon, is simulated. The predicted spread of $CO_2$ agrees (qualitatively) very well with the observations. The method provides a means of determining a potential 'safe height' above which simulated concentrations are not hazardous, and thus the height above which refuge should be taken during similar future events. The simulation demonstrates a novel application which can be rapidly applied to other scenarios.

KEY WORDS dense gas; forecasting; gravity current; hazards; modelling; WRF

*Received 8 June 2015; Revised 28 June 2016; Accepted 29 June 2016*

## 1. Introduction

The spread of dense gases, or particle–gas mixtures that can be treated as gas mixtures, is a phenomenon that occurs widely in nature: for example, volcanic degassing and volcanic pyroclastic flows (Sparks *et al*., 1997) and the movement of dust-rich air masses (e.g. West African frontal systems, Burton *et al.*, 2012). Anthropogenic releases of potentially harmful dense gases have motivated the development of numerous models (see for example Duijm *et al*., 1997). The release of dense gases in such cases, whether natural or anthropogenic, is generally hazardous (or at least of high impact) in relation to human wellbeing and safety: for example the Bhopal disaster of 1984 where an accidental release of methyl isocyanate from the Union Carbide pesticide plant in India caused as many as 20 000 deaths (Varma and Varma, 2005).

The ability to simulate a dense gas release is commonly performed by the use of several models, of increasing complexity. The following classification is derived from Duijm *et al*. (1997): (1) phenomenological models; (2) 1D integral models or box models; (3) models based upon shallow-layer equations; and (4) models based upon the full 3D Navier–Stokes equations. More complex computational fluid dynamics models have been developed that can incorporate the effects of topography and demonstrate how this is beneficial (Scargliali *et al*., 2005). The following study shows for the first time how dense gases may be represented in a state-of-the-art numerical weather prediction (NWP) model with a minimum of alterations to the NWP software. In addition to the sophisticated representation of physical processes such as turbulence, radiative and microphysical effects, and the use of state-of-the-art numerical schemes, NWP models allow the use of fully time-varying meteorological fields and have the ability to simulate gas releases on scales from metres to kilometres. The model used is the Weather Research and Forecasting (WRF) model version 3.5.1 (Skamarock *et al.*, 2008; WRF, 2015). Currently used in over 130 countries and with over 25 000 registered users (WRF, 2015), WRF is an open-source model that can run on desktop PCs or multiple-processor machines, depending upon the complexity of the required simulation. One of the principal advantages of the WRF, particularly with regard to the present application, is that it can be implemented at scales from tens of metres to thousands of kilometres, from city scale to continental scale (Fernando, 2012). All the results in the following study used an eight-processor desktop machine.

## 2. Model configuration and testing

The means of introducing the dense gas into the WRF configuration is straightforward. An extra mixing ratio $q_{\text{gas}}$, associated with the dense gas, is included in the model. (Technically, the extra mixing ratio is carried with the microphysics mixing ratios but does not interact with the microphysics *per se*, and all microphysical processes are computed as they would be in the absence of $q_{\text{gas}}$.) The addition of dense gas can be looked upon as keeping the number of molecules in a reference volume constant, replacing $O_2$ molecules (for example) with dense gas molecules, one for one, and thus changing the mass in the reference volume. However, for ease of implementation, the gas constant in the reference volume is not modified, and so the pressure remains unchanged (from the equation of state in the form $PV = nRT$, where $n$ is the number of molecules). Of course, in reality the gas constant would change, consequently adding a source of potential temperature; this effect (estimated to be a small fraction of the buoyancy difference associated with the addition of

* Correspondence: R. R. Burton, NCAS, University of Leeds, LS2 9JT, UK. E-mail: ralph.burton@ncas.ac.uk

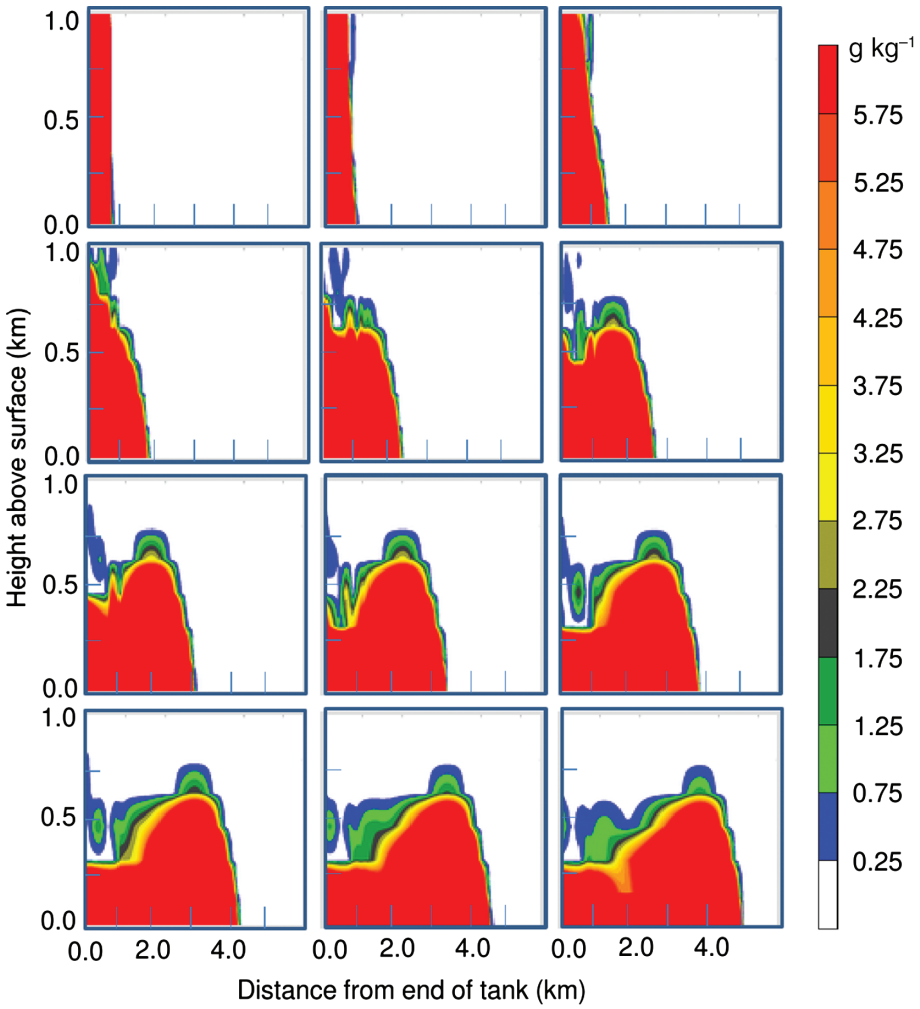


Figure 1. Concentrations of dense gas (colour shaded, g kg$^{-1}$) at successive times for the dam-break test case. Plots are valid (left to right, top to bottom) for 5, 25, 50, 75, … , 275 s after lock removal. The actual domain extends to 150 km in the lateral direction.

$CO_2$) has been neglected. This requires minimal alteration to the code due to the WRF software compilation features (in particular, the 'Registry' feature which allows simple code manipulation and addition of extra variables). The addition of an extra microphysical mixing ratio acts to reduce the buoyancy (indeed, can make the buoyancy negative) at certain points corresponding to the dense gas 'release'. The gas can then be initialized for an instantaneous, continuous or time-dependent release. It should be stressed that using this approach the atmospheric flow affects the dense gas and, importantly, *vice versa* (unlike chemical transport models or coupled meteorology−chemistry models, e.g. the chemistry version of WRF, WRF-CHEM). Currently, this approach is applied to gases that remain in the gas phase; complex chemical and thermodynamic processes, such as condensation of the gas, are not considered.

As a test case an idealized simulation of fluid release in a channel is carried out: the 'dam-break' (Rottman and Simpson, 1983; Simpson, 1997). Here, $CO_2$ gas with a mixing ratio of 6 g kg$^{-1}$ is confined in a channel with height 1 km, lock-length 1 km and channel length 150 km (see Figure 1). This channel length was chosen so as to eliminate any potential effects from the downstream boundary. There are no background winds; the stratification is neutral below 1 km and follows the US standard atmosphere above 1 km altitude. The horizontal resolution is 100 m resolution, with 140 points in the vertical (variable resolution, but seven levels below 1 km). This two-dimensional implementation has no surface friction, radiation or microphysical effects, and no boundary-layer parametrization. The left-hand lateral boundary is a 'wall' condition; the right-hand lateral boundary is open.

The lock is instantaneously released. As can be seen (Figure 1), the collapse of the gas column appears qualitatively similar to laboratory flow-tank releases (snapshots of which can be seen in, for example, Simpson, 1997) with a well-defined head region. Figure 2 shows the position of the gas front against time. In the initial stages the front speed is nearly constant, until it has travelled approximately five lock-lengths or 2500 m. After this there is a transition zone; subsequently, the front speed propagates according to $x \sim t^{0.67}$.These results agree very well with theoretical and laboratory results. Rottman and Simpson (1983) describe such 'dam-break' flow speeds as being 'approximately constant (actually, very slowly decreasing)' for the first few lock-lengths with the front location following a $t^{2/3}$ power law at later times (the latter relationship coming from shallow-water equations; the 'self-similar' phase). Rottman and Simpson (1983) estimated that for small $h/H$ (where $h$ is the height of dense fluid and $H$ is the height of the tank, or atmosphere in this case) the 'constant speed' regime should continue for approximately three lock-lengths; this agrees well with the results shown here. Note that the flow in these simulations is determined by the inertia: viscous effects would only become evident after the front has

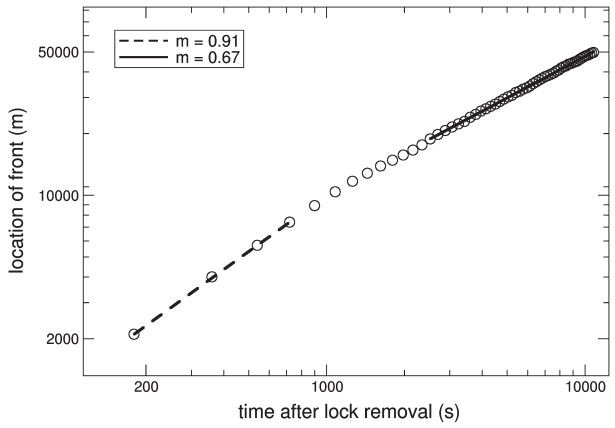


Figure 2. Distance from the lock-release point against time (open circles) for test gas release in the dam-break analogy. The two solid lines show gradients of 0.91 and 0.67, corresponding to two regimes during the spread of fluid. Correlation co-efficients for the two regression lines are both greater than $r = 0.99$.

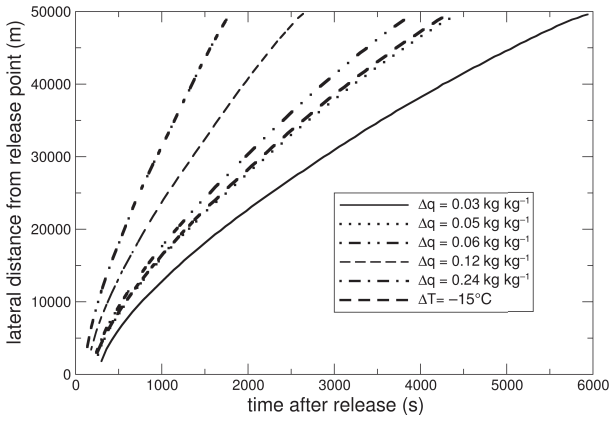


Figure 3. The surface spread of gravity currents with time for bubbles of various density perturbations (solid lines) and the standard Weather Research and Forecasting model thermal perturbation of −15 °C (heavy dashed line, conforming to the Straka *et al.* (1993) test case: see text). The lines show the lateral distance of the head of the gravity current at the surface from the initial centre of the bubble, i.e. the distance from the release point. The bubble configuration is described in the text.

travelled approximately 300 km (Simpson, 1997, equation (4.1)), well beyond the domain sizes presented here. The height of the simulated front at the leading edge (not shown) also agrees very well with Rottman and Simpson (1983) for the $h/H \to 0$ case.

The case of a gravity current in a resting isothermal atmosphere, due to the release of an upper level cold bubble, is a relatively well studied case (Straka *et al*., 1993). The falling bubble assumes the form of a vortex-type structure which spreads laterally upon impact at the ground. WRF has been subjected to numerous tests to reproduce gravity currents from this benchmark (Skamarock, 2013). The cold bubble is defined in Straka *et al*. (1993) and is centred at 3 km altitude above flat ground with a maximum temperature perturbation inside the bubble of $\Delta T = -15\,^{\circ}\mathrm{C}$; it then falls to the surface and the subsequent lateral motion is tracked. Here, this test has been repeated with a dense $CO_2$ (instead of cold air) bubble, the dense bubble being morphologically similar to a cold bubble, and the results are shown in Figure 3 which shows the position of the head of the gravity current with time. The resolution used is 100 m in the horizontal and variable resolution in the vertical (as described above for the lock-release case). It can be seen that the denser the gas the more rapidly the gravity current spreads laterally at the surface. A dense bubble with a maximum mixing ratio perturbation of $\Delta q = 50\,\mathrm{g\,kg^{-1}}$ can be constructed that effectively mimics the behaviour of the cold bubble.

It is also instructive to examine the model response in the case of a stratified atmosphere. In the following tests the atmosphere is stratified with a surface temperature of 300 K and an increase of $5\,\mathrm{K\,km^{-1}}$ altitude. The cold bubbles and dense bubbles are constructed so that the buoyancy force $F_B$ is the same in each case:

$$F_B = g\frac{\rho - \rho_0}{\rho_0} = g\frac{T_0 - T}{T}$$

where $\rho$ and $T$ are the bubble density and temperature respectively and the subscript 0 refers to the ambient state. Bubble positioning and structure are the same as in the neutral-atmosphere cases studied above. To facilitate comparison between the two runs, a passive (non-dense) tracer is also added, whose value is proportional to the density or temperature perturbation and is identically distributed in the two cases at initialization (Figure 4(a)). At successive times (left-hand panels in Figures 4(b) and (c)) the concentrations in the two cases follow a broadly similar pattern, with both bubbles descending and spreading laterally; indeed, they are visually very similar. Closer inspection, however, shows that there are differences: the dense bubble has higher (than the cold bubble case) concentrations at lowest levels (the red/brown regions in the right-hand panels in Figure 4). The cold bubble is more evenly distributed in the vertical, with higher (than the dense bubble case) concentrations confined in a layer 1 km above the surface (the green regions in the right-hand panels in Figure 4). With respect to the subsequent atmospheric stratification (Figure 5), the dense bubble produces a quasi-static, highly stable region close to the surface due to warm air being brought down by the dense gas that is able to stay there and is compensated by the negative density, whereas the cold bubble case produces an essentially wavelike response throughout the atmosphere as it returns to the original stratification.

Further work would be needed to fully determine the effect of stratification upon the release of dense bubbles but the above shows that, in a stratified atmosphere, there is a difference between the behaviours of a dense and of a merely cold bubble. The daytime situation would also be rather different, as a positive surface heat flux could make the dense layer less negatively buoyant but would not remove the negative buoyancy.

The above tests show that the present configuration agrees with the well tested suite of gravity current tests that have been developed for WRF; it also agrees with theoretical predictions and laboratory studies and can be used for novel experimental investigations.

## 3. Application to the Lake Nyos disaster, 1986

The Lake Nyos disaster in Cameroon, 1986 (Sigurdsson, 1983; Kling *et al*., 1987), saw a large, dense, $CO_2$ cloud rapidly emerge from Lake Nyos (by a process of limnic eruption) and spread into the surrounding areas: the concentrations of $CO_2$ released were such that over 1700 fatalities occurred in a very short time. The event occurred at 2100 UTC on 21 August 1986. The disaster has been previously modelled using a shallow water approach (Costa and Chiodini (2015), hereafter CC15, who also provide many references to the event).

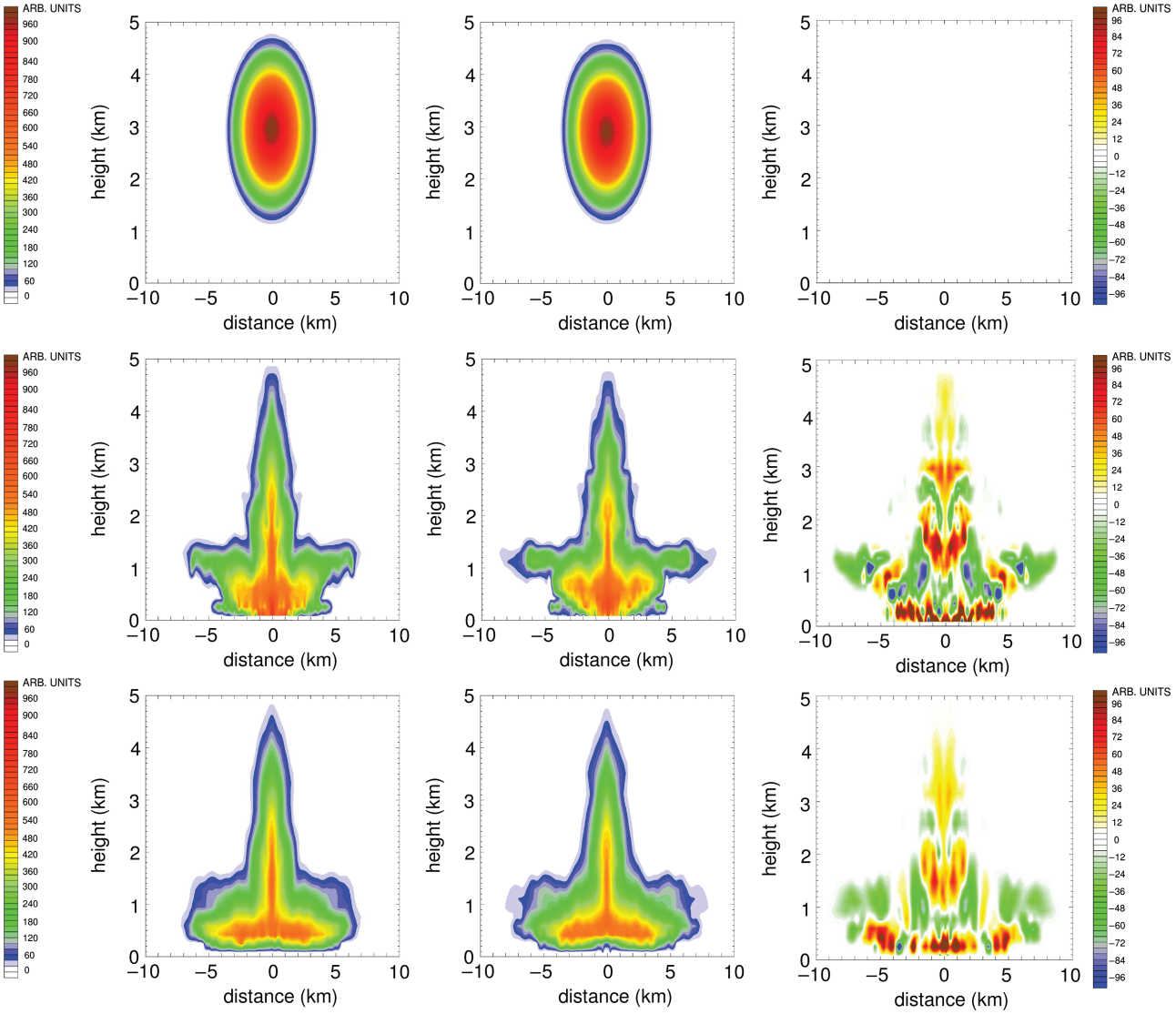


Figure 4. (a) Concentration (arbitrary units, colour-shaded) for the dense bubble ($C_\rho$, left-hand panel), the cold bubble ($C_\theta$, middle panel) and the difference $C_\rho - C_\theta$ (right-hand panel) at initialization; (b), (c) as for (a) but after 1 h (b) and 2 h (c) of simulation. Only a portion of the domain is shown. The colour bar at the extreme left refers to the concentrations; the colour bar at the extreme right refers to the difference in concentrations.

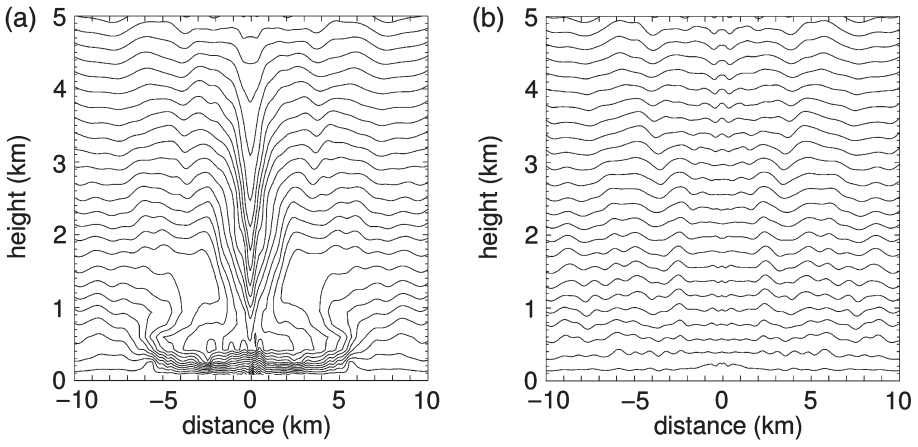


Figure 5. Potential temperature (1 K contour intervals) after 2 h of simulation for (a) the dense bubble and (b) the cold bubble. Only a portion of the domain is shown.

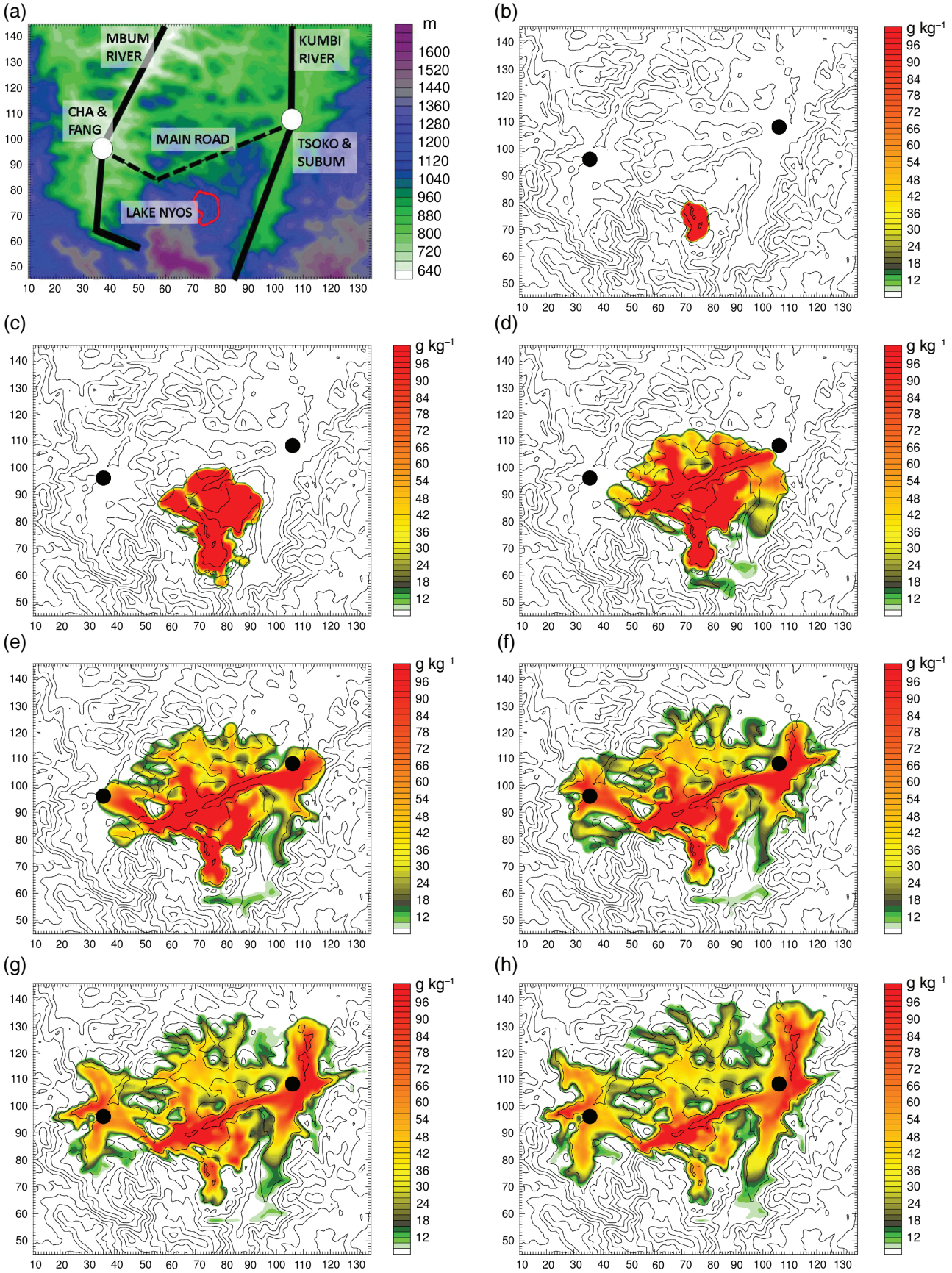


Figure 6. (a) The geography and topography of the Lake Nyos region showing heights above mean sea level (colour shaded). The domain size is 20 km (north–south) × 25 km (west–east). Axis tick points represent model gridpoints. (b) Spread of $CO_2$ at the lowest model level for 5 min after release. Axis labelling as in (a). Topography is shown every 100 m and the village groups are identified by solid circles. (c)–(h) As for (b) but for 10, 15, 20, 25, 30, 35 min after release.

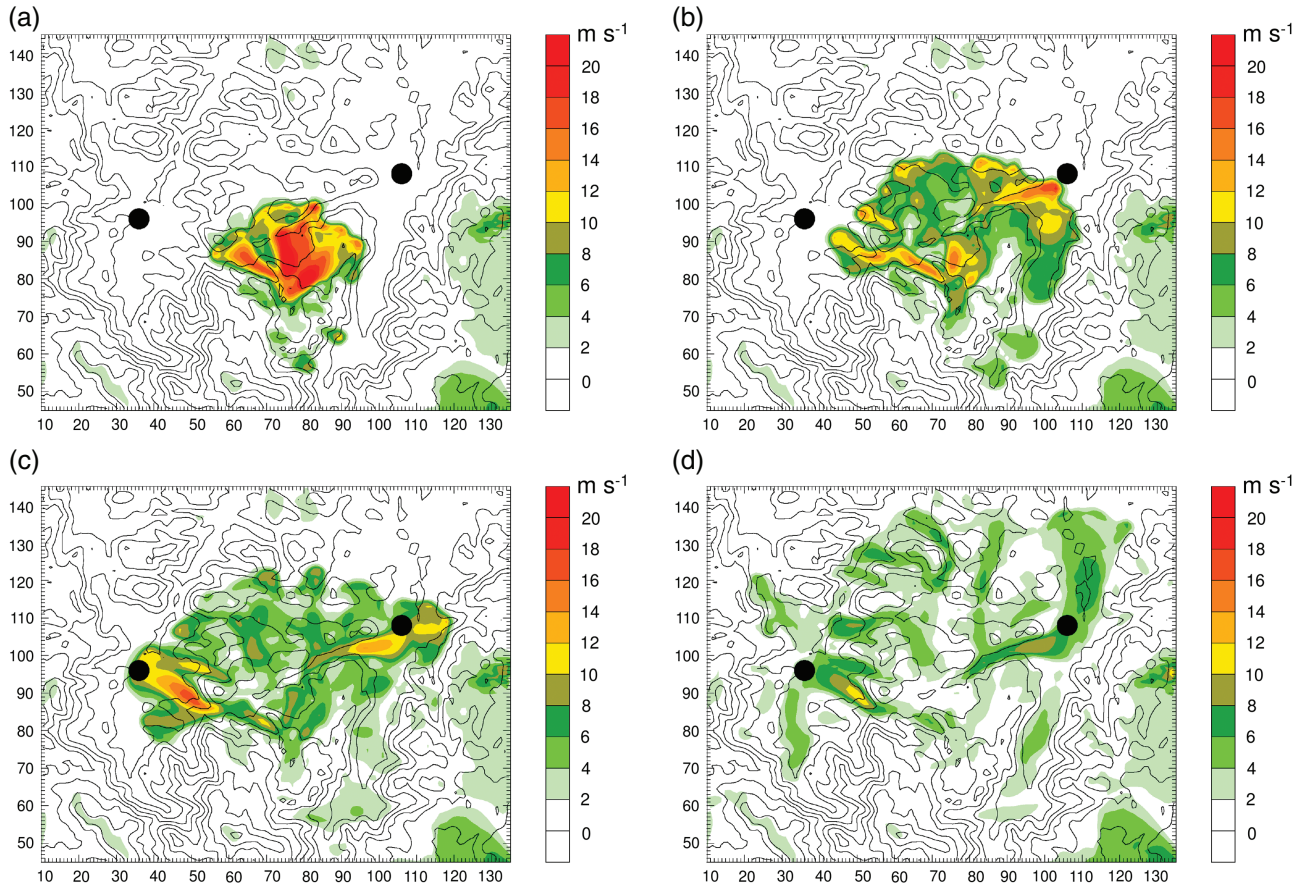


Figure 7. As for Figure 6, but wind speeds (colour shaded) at the lowest model level for (a) 10 min, (b) 15 min, (c) 20 min and (d) 30 min after release. Topography is shown as solid contours (contour spacing 100 m). The domain size is 20 km (north–south) × 25 km (west–east). Axis tick points represent gridpoints; gridpoint separation is 200 m. Village groups are denoted by solid circles.

To simulate this event, the model was initialized with National Center for Atmospheric Research/National Center for Environmental Prediction (NCAR/NCEP) reanalyses (Kalnay *et al*., 1996) for 21 August 1986. The topography data used are nominally 90 m in resolution (Consultative Group on International Agricultural Research-Consortium for Spatial Information, 2014), capable of representing the complex topography of the region (see Figure 6(a)). The model domain is 30 km × 30 km (200 m resolution) with 71 terrain-following vertical levels (of varying resolution; of the order of 100 m in the lowest 1 km above ground level (AGL), with the first and second model levels at 30 and 100 m AGL respectively). Operational implementations of this technique may require model levels closer to the ground, but the 30 and 100 m levels were deemed sufficient for the present demonstration of the method. Model physics included a 3D turbulence kinetic energy (TKE) based subgrid turbulence scheme. This uses second-order horizontal diffusion on model surfaces, preventing diffusion up and down valley sides, and acting on full (not perturbation) fields. Vertical diffusion is computed *via* a 1.5-order TKE scheme. For a detailed description of the subgrid scale TKE scheme see Skamarock *et al.* (2008). The effects of strong stratification in suppressing vertical mixing is an important research topic. Basu and Porté-Agel (2006) highlighted that subgrid scale schemes still have problems with vertical mixing. Further tests would be required to fully explore the dependence upon stratification. However, a more complete TKE buoyancy-term treatment is unlikely to affect the resolved motion significantly. Additionally, a thermal diffusion land-surface scheme with four soil levels, a Monin–Obukhov based surface layer scheme and a Morrison double-moment microphysics scheme were implemented. All these schemes are standard in WRF, and further details may be found in Skamarock *et al.* (2008). Due to the large wind speeds simulated (see below), a time step of 0.5 s was required to avoid Courant–Friedrichs–Lewy violation.

The simulation was started at 1800 UTC on 21 August, and the release started the same day at 2100 UTC, in a model location conforming to the lake area (Figure 6(a)). Although the exact nature of the gas release will never be known, estimates have suggested (Kling *et al*., 1987) that the gas cloud extended approximately 100 m (i.e. in the lowest two model levels in this simulation) above the lake. The modelled release lasted for 5 min duration (in accordance with the description of the release as 'sudden [and] catastrophic', Kling *et al*., 1987) and stopping thereafter.

Defining the mixing ratio of $CO_2$ in dry air as $q$ g kg$^{-1}$, then $q = 10^{-3}\, PR_{\mathrm{air}} m/M$ where $P$ is concentration in parts *per* million by volume, $R_{\mathrm{air}}$ is the specific gas constant for dry air, $m$ is the molar mass of $CO_2$ and $M$ is the molar gas constant (equivalent to multiplying by the ratio of molecular weights). The mixing ratio of the initial cloud is taken to be 480 g kg$^{-1}$, corresponding to a $CO_2$ concentration of approximately 37% by volume, of the same order of concentration as reported during similar hazardous occurrences (International Volcanic Health Hazard Network, 2015). Of course the exact concentration of $CO_2$ released during this event is unknown, but concentrations of $CO_2$ above 8%

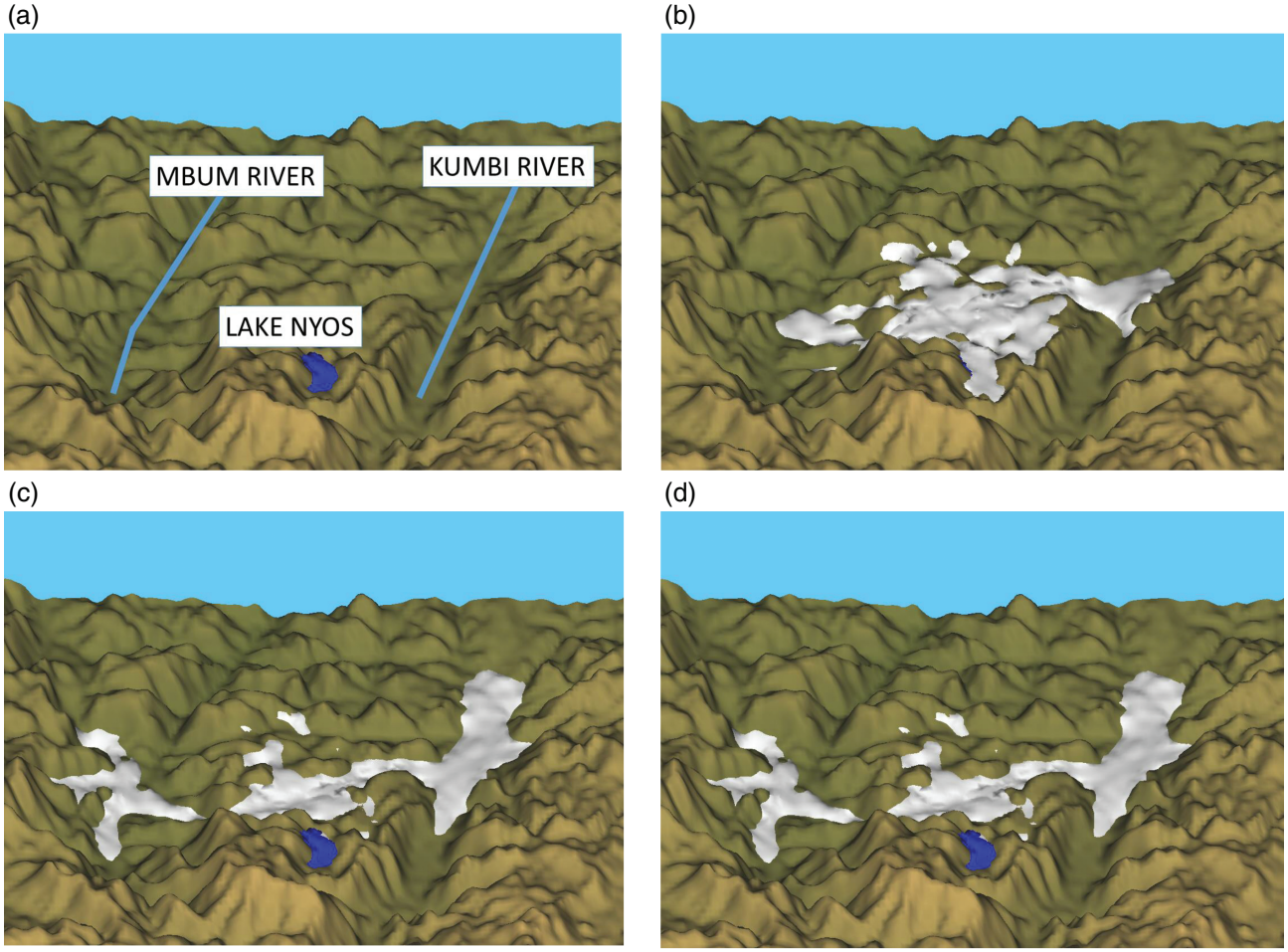


Figure 8. Three-dimensional visualization of the simulated spread of $CO_2$ from Lake Nyos. (a) Before eruption and (b) 20, (c) 40 and (d) 60 min after eruption. The 5% $CO_2$ concentrations in all plots represent the threshold level where the onset of laboured breathing occurs. The plots are designed to simulate a viewpoint from an elevated position, looking due north.

can be lethal to humans (International Volcanic Health Hazard Network, 2015).

As can be seen (Figure 6) the $CO_2$ moves to the north and flows down the two main river valleys, reaching the two village groups in approximately 20 min (agreeing with the results of CC15). The rapid advance of the gas cloud (Figure 7), with speeds in excess of 20 m s$^{-1}$ at the leading edge, is consistent with Sigurdsson (1983): 'Within a few km of the lake, the density and velocity of the gas flow was sufficient to flatten vegetation, such as corn stalks, banana plants and some trees, consistent with the behaviour of the flow as a density current'. These simulated values are slightly higher those predicted by the von Kármán (1940) type solution:

$$U = \sqrt{\left(\frac{\Delta\rho}{\rho}\right) gH} \sim 12m\ \ s^{-1}$$

where $U$ is speed, $\Delta\rho$ is density perturbation ($\rho$ being the density of unpolluted air) and $H$ is the height of the dense fluid. However, this theoretical treatment does not take into account the complicating factors of the non-uniform slopes and associated flow channelling prevalent in this region, nor the background wind speeds, shear and thermal stratification.

After 20 min of simulation, high $CO_2$ concentrations are simulated in the principal villages of Cha, Subum, Fang and Nyos (see Figure 6(e)). Again, this is entirely consistent with reality: these villages together suffered over 1700 fatalities during this episode. The lowest model level concentrations in the To/Cha and Tsoko/Subum village regions after 30 min are above 100 g kg$^{-1}$ (8% $CO_2$) which can cause death unless oxygen is administered immediately (International Volcanic Health Hazard Network, 2015). At successive times, as the cloud dissipates, the speed of spread decreases; in particular, the speeds along the main road to the north of Nyos are generally low, leading to an accumulation of gas in that region. Accumulation, or pooling, of $CO_2$ is also evident in other valley systems, as shown in Figure 8; in particular, the Kumbi river valley has a significant accumulation, associated with the steep slopes on either side of the valley. It should be noted that dangerous levels of $CO_2$ in the Kumbi river valley are apparently absent in the results of CC15, for all scenarios considered by them. Sigurdsson (1983) shows (his figure 3) $CO_2$ in the Kumbi river valley and fatalities were indeed reported there (CC15, their figure 5). Differences in results between the present work and those of CC15 would require further study but are likely to be linked to the meteorological initialization and the full physics used here. Apart from the absence of $CO_2$ in the Kumbi valley, the present results are qualitatively similar to CC15, especially their scenario III.

It should be emphasized that the resultant simulated accumulations of gas will depend upon the (in reality unknown) concentration and volume of the initial cloud (as demonstrated in CC15).

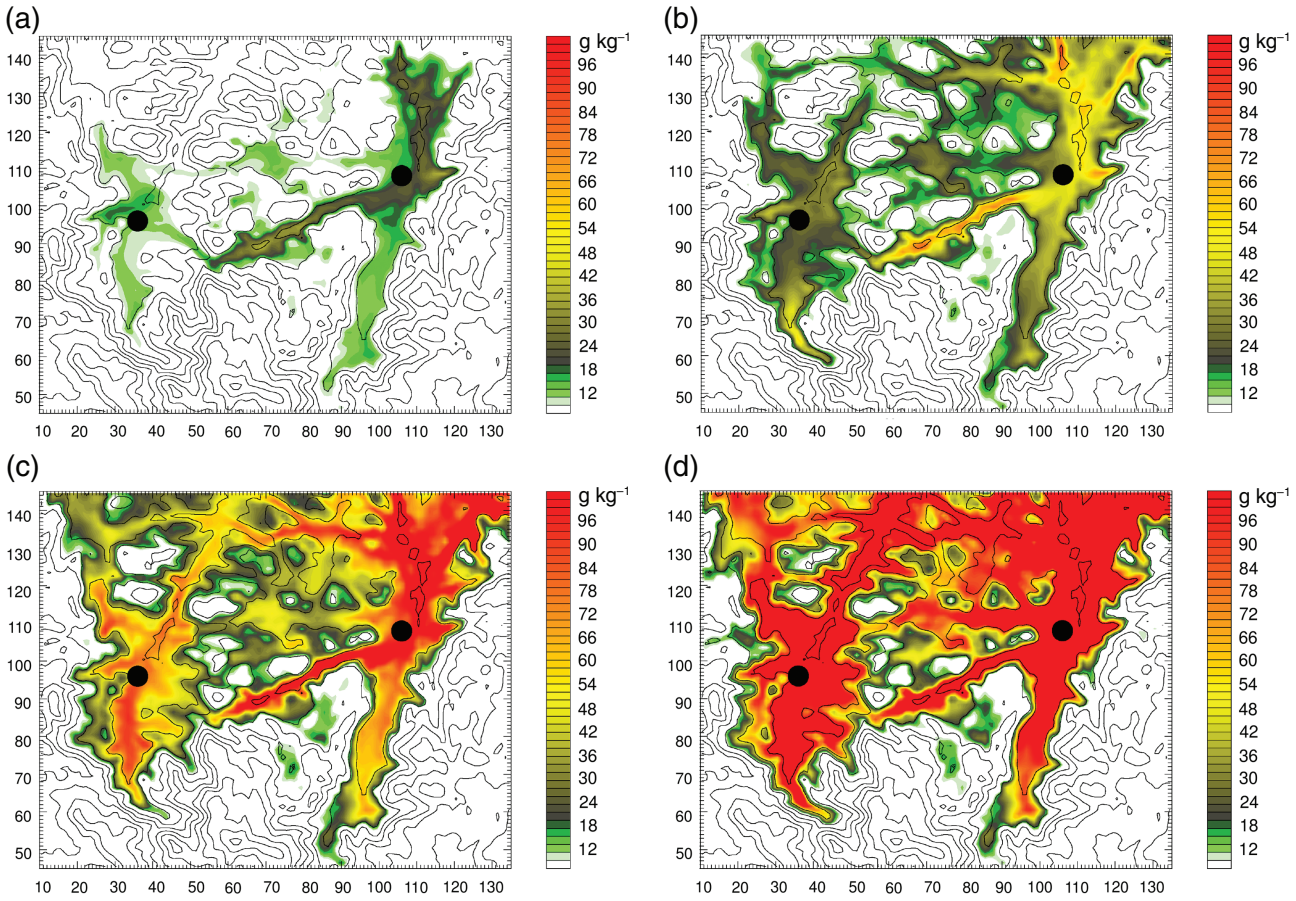


Figure 9. (a) As for Figure 6 but 1 h after release, for initial cloud concentrations of (a) 120, (b) 240, (c) 480 and (d) 960 g kg$^{-1}$.

To somewhat mitigate this deficiency, the model has been run with different initial concentrations (from 120 to 960 g kg$^{-1}$, the latter value being approximately 95% $CO_2$ by volume) and the results are shown in Figure 9. As can be seen a similar pattern is found in all runs, with the principal accumulations along the main road and along the two river valleys, agreeing very well with the observed locations of the gas and the associated fatalities (Sigurdsson, 1983, figure 3).

The dependence of concentration upon height is an important matter, as it can lead to predicting a height above which concentrations are low or sufficiently low to escape the worst effects of gas poisoning. Figure 10 shows that, in general, the highest concentrations occur at lowest elevations with an apparently exponential dependence of concentration upon height (several regimes are apparent in this figure, coinciding with the main valley systems). Based on these simulations, 1300 m above mean sea level (AMSL) would have been a 'safe' altitude; above this height (the blue areas in Figure 4(a)), concentrations were zero. In contrast, potentially lethal concentrations are found at heights below 950 m AMSL (the green and white areas in Figure 6(a)). The latter height equates to a height of 300 m above the valley containing the Mbum river and 100 m above the valley containing the Subum river. Importantly, these 'safe heights' apply to all the initial cloud concentrations studied here. Further work (using differing meteorological forcings and source terms) would confirm the generality of these safe heights, and this might be of help in preventing future fatalities. Since 2005, mechanisms have been put in place to slowly release $CO_2$ from the lake (BBC News, 2005) and so perhaps prevent future catastrophic releases.

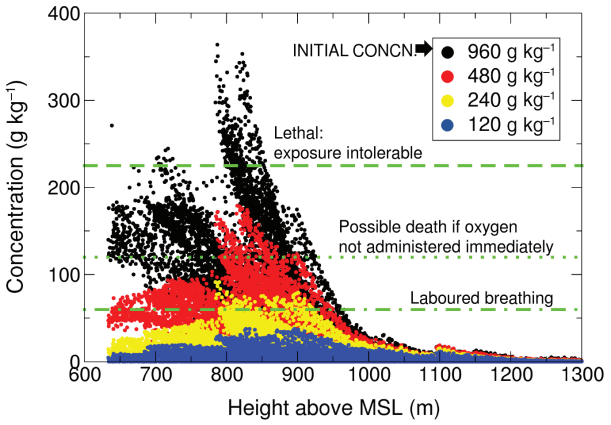


Figure 10. Concentrations of $CO_2$ with height, 1 h after release, for various initial cloud concentrations. Important concentration thresholds are marked.

## 4. Summary

In the present study a straightforward, easily implemented means of treating dense gases in a numerical weather prediction (NWP) model is presented. The model is tested against laboratory studies and existing NWP test cases. This study has demonstrated an application of the Weather Research and Forecasting model as an efficient tool in the modelling of dense gas dispersion.

In a real-life application, the simulation of the Lake Nyos disaster shows that the modelled spread of a gas cloud bears a very good resemblance to the observations. The quantitative element, of course, is subject to a large degree of uncertainty, given the lack of knowledge regarding initial conditions. Additionally, the model cannot represent very complex phenomena such as the storage, expansion and cooling of $CO_2$ as it passed from Lake Nyos to the atmosphere. However, it is clear that the model does a very good job of predicting the subsequent spread of the dense gas and provides a means of estimating the lowest altitudes that may be considered safe in the event of a similar occurrence. It is feasible that many likely scenarios (differing wind directions, for example) for this location could be simulated to construct a map of geographical locations which are likely to be impacted by a dense gas release. Additionally, if building scale features do not need to be resolved, the method could be used to predict the spread of an accidental release from a chemical plant, e.g. the Bhopal disaster mentioned in Section 1.

## Acknowledgements

Burton, Gadian and Mobbs are funded by the UK Natural Environment Research Council. Dudhia is funded by the US National Science Foundation through the University Corporation for Atmospheric Research. The authors would like to thank the two anonymous reviewers whose suggestions and comments have improved this paper.

## References

Basu S, Porté-Agel F. 2006. Large-eddy simulations of stably stratified atmospheric boundary-layer turbulence: a locally averaged scale-dependent dynamic modelling approach. *J. Atmos. Sci.* **63**: 2074–2091.

BBC News. 2005. Action needed on deadly lakes. http://news.bbc.co.uk/1/hi/sci/tech/4285878.stm (accessed 28 April 2015).

Burton RR, Devine GM, Parker DJ, Chazette P, Dixon N, Flamant C, et al. 2012. The Harmattan over West Africa: nocturnal structure and frontogenesis. *Q. J. R. Meteorol. Soc.* **139**: 1364–1373.

Consultative Group on International Agricultural Research-Consortium for Spatial Information. 2014. SRTM 90 m Digital Elevation Database v4.1. http://srtm.csi.cgiar.org/SELECTION/inputCoord.asp (accessed 28 April 2015).

Costa A, Chiodini G. 2015. Modelling air dispersion of $CO_2$ from limnic eruptions. In *Volcanic Lakes*, Rouwet D, Christenson B, Tassi F, Vandemeulebrouck J (eds). Springer-Verlag: Berlin; 451–465.

Duijm NJ, Carissimo B, Mercer A, Bartholme C, Giesbrecht H. 1997. Development and test of an evaluation protocol for heavy gas dispersion models. *J. Hazard. Mater.* **56**: 273–285.

Fernando HJS (ed). 2012. *Handbook of Environmental Fluid Dynamics, Volume 2: Systems, Pollution, Modeling, and Measurements*. CRC Press: Boca Raton; 352.

International Volcanic Health Hazard Network. 2015. Carbon dioxide. http://www.ivhhn.org/index.php?option=com_content&view=article&id=84 (accessed 28 April 2015).

Kalnay E, Kanamitsu M, Kistler R, Collins W, Deaven D, Gandin L, et al. 1996. The NCEP/NCAR 40-year reanalysis project. *Bull. Am. Meteorol. Soc.* **77**: 437–471.

von Kármán T. 1940. The engineer grapples with nonlinear problems. *Bull. Am. Math. Soc.* **46**: 615–683.

Kling GW, Clark MA, Compton HR, Devine JD, Evans WC, Humphrey AM, et al. 1987. The 1986 Lake Nyos gas disaster in Cameroon, West Africa. *Science* **236**: 169–175.

Rottman JW, Simpson JE. 1983. Gravity currents produced by instantaneous releases of a heavy fluid in a rectangular channel. *J. Fluid Mech.* **135**: 95–110.

Scargliali F, Di Renzo E, Ciofalo M, Grisafi F, Brucato A. 2005. Heavy gas dispersion modelling over a topographically complex mesoscale: a CFD based approach. *Trans. IchemE, B: Process Saf. Environ. Prot.* **83**(B5): 1–16.

Sigurdsson H. 1983. Gas bursts from Cameroon Crater Lakes: a new natural hazard. *Disasters* **12**: 131–146.

Simpson JE. 1997. *Gravity Currents in the Environment and the Laboratory*. Cambridge University Press: Cambridge.

Skamarock B. 2013. Initialization for idealized cases. www2.mmm.ucar.edu/wrf/users/tutorial/201301/wang_idealized.pdf (accessed 28 April 2015).

Skamarock W, Klemp JB, Dudhia J, Gill DO, Barker D, Duda MG *et al.* 2008. A description of the advanced research WRF version 3. NCAR Technical Note NCAR/TN-475+STR, National Center for Atmospheric Research: Boulder, CO.

Sparks RSJ, Nursik MI, Carey SN, Gilbert JS, Glaze LS, Sigurdsson H, et al. 1997. *Volcanic Plumes*. Wiley: Chichester, UK.

Straka JM, Wilhelmson RB, Wicker LJ, Anderson JR, Droegemeier KK. 1993. Numerical solutions of a non-linear density current: a benchmark solution and comparisons. *Int. J. Numer. Methods Fluids* **17**: 1–22.

Varma R, Varma DR. 2005. The Bhopal disaster of 1984. *Bull. Sci. Technol. Soc.* **25**: 37–45.

WRF. 2015. The weather research and forecasting model. www.wrf-model.org/index.php (accessed 28 April 2015).